OLDROYD-B NANOFLUID-FLOW BETWEEN STRETCHING DISKS WITH THERMAL SLIP AND MULTIPLE FLOW FEATURES

by

Ilyas KHAN[a], Sami ULLAH KHAN[b], Yu-Ming CHU[c,d], Kottakkaran Sooppy NISAR[e*], and Kamel AL-KHALED[f]

[a] Faculty of Mathematics and Statistics, Ton Duc Thang University, Ho Chi Minh City,Vietnam
[b] Department of Mathematics, COMSATS University Islamabad, Sahiwal, Pakistan
[c] Department of Mathematics, Huzhou University, Huzhou, China
[d] Hunan Provincial Key Laboratory of Mathematical Modelling and Analysis in Engineering, Changsha University of Science and Technology, Changsha, China
[e] Department of Mathematics and Statistics, Jordan University of Science and Technology, Irbid, Jordan
[f] Department of Mathematics, College of Arts and Sciences, Prince Sattam binAbdulaziz University, Wadi Aldawaser, Saudi Arabia

Original scientific paper
https://doi.org/10.2298/TSCI20S1083K

This novel investigation deals with the thermal slip in magnetized axi-symmetric flow of Oldroyd-B liquid configured by infinite stretchable disks. With appliance of fundamental laws, the flow model equations are constructed. The governing flow equations are altered into no-dimensional form by using similarity quantities. The solution procedure is followed by using famous homotopy analysis technique. The convergence analysis is performed to evaluate the solution accuracy. The significance of flow parameters in the pattern of velocity, temperature and concentration are graphically illustrated. The novel numerical simulations for wall shear stress, Nusselt number, and Sherwood number are also performed at both surfaces of disks. It is noted the effects of relaxation time and retardation constants on radial and normal velocity components is opposite. The thermal slip parameters enhance the nanoparticles temperature. The concentration profile is decreases with Brownian motion parameter.

Key words: *Oldroyd-B fluid, stretching disks, slip flow, magnetic field, homotopy analysis method*

Introduction

Recently, the dynamic interest of researchers is developed towards the flow simulations induced by stretchable disks which include the applications of semi-conductors, rotating wafers, suction flow modelling, viscometer, diffusers, geothermal engineering, thrust bearings, biomechanics, power transmission, *etc.* The micro-devices structured on the disks applications allow various types of fundamental applications in biomedical, surgical apparatus, micro-channels, motors, pumps, electronic cooling, *etc.* The fundamental investigation on flow induced by stretchable disks was pioneered by Karman [1] which provides a direction many investigators to work on this topic. Many investigators studied the disk flow phenomenon under various flow conditions and diverse flow features. For instance, Hayat *et al.* [2]

* Corresponding author, e-mail: n.sooppy@psau.edu.sa, chuyuming@zjhu.edu.cn

utilized the modified heat and mass flux expressions to explore the heat transfer phenomenon for third grade liquid configured by starching disks. The stagnation point analysis for hydromagnetic-flow between stretching disks was numerically focused by Turkyilmazoglu [3]. In another investigation, Turkyilmazoglu [4] examined the features of heat transfer in asymmetric flow of viscous material induced by shrinking and rotating disk. The magnetic field features for viscous fluid-flow between convectively heated disks was worked out by Soid *et al.* [5]. The utilization of nanoparticles in Newtonian fluid for uniformly moving disks was intended by Yin *et al.* [6]. Some interesting numerical simulations for flow problem induced by stretchable disks has been focused by Turkyilmazoglu [7]. The mixed convection impact for flow of Oldroyd-B material in isothermal moving disks was analyzed by Hashmi *et al.* [8]. Rashidi *et al.* [9] examined the slip features while examining the diffusion-thermo aspects in stretching disks. Khan *et al.* [10] find out the analytical solution for disk flow of viscous fluid by following convergent procedure. In another analysis, Khan *et al.* [11] reported the joule heating and viscous dissipation aspects in axi-symmetric flow encountered by stretching disks.

The investigation regarding the flow of non-Newtonian materials is another attracting research area in recent century due to their novel industrial, engineering and daily life applications. The non-Newtonian fluid possessed non-linear interaction shear stress and warping change. The prime reason behind such motivating attention of researchers towards the non-Newtonian fluid is justified due to their prestigious applications in the chemical industries, engineering processes, medical applications, food industries, mechanical sciences, processing industries and many more. The complicated rheological consequences of such materials insisted the scientists to suggest unqiue relationship for each non-Newtonian fluid model. Among various proposed fluid models, Oldroyd-B fluid one the most interesting and useful non-linear model which successfully allow to examine the important relaxation and retardation features. This model is characterized to the rate type fluids and presents the results for Maxwell fluid and viscous material as a limiting case. Owing to these valuable properties of Oldroyd-B fluid, many researchers used this model under different circumstances. For instance, Zheng *et al.* [12] reported the hydromagnetic-flow of Oldroyd-B liquid over an accelerating surface. The stretched flow of Oldroyd-B fluid has been reported by Hayat *et al.* [13]. They adopted convergence algorithm to communicate the solution procedure. The modelling for fractional type of Oldroyd-B under the impact of slip was led by Zheng *et al.* [14]. The flow Oldroyd-B fluid under the creeping constraints with applications of DLM simulations has been notified by Chiu *et al.* [15]. Farooq *et al.* [16] thrashed out the major consequences of Oldroyd-B fluid analytically.

The fluid-flow under the influence of magnetic force reports many narrative applications and studied by many investigators in recent years. The implications of magnetic field for such liquids flow provide us to avert the uncertain deviations of viscosity lubrications with temperature in the operational conditions of extreme type. The MHD has key applications in physics, chemistry, engineering and mathematics such as cancer therapy, strips cooling, power generation, drug delivery, nuclear plants, safer surgery, sample mixing, tumor elimination, MHD pumps gastric medication, sterilized devices, biological transportation*, etc.* Some recent investigations for various fluid-flow under the impact of magnetic field can be seen in references [17-24].

After carefully evaluating the aforementioned literature survey, aim here to report the heat and mass transportation for flow of Oldroyd-B nanofluid confined by stretching and rotating disks. The Brownian motion and thermophoresis aspects are taken into consideration. The flow is subjected to the magnetic force. The thermal slip features are utilizes to explore the thermal performances of non-Newtonian fluid. It is remarked that some studies are already

available in the literature regarding flow due to stretching disks but velocity and thermal slip features in flow of Oldroyd-B nanofluid is not reported yet. In order to fill this research gap, present communication is reported. The governing equations are modeled and then retained dimensional forms. The analytical solution is computed with appliance of homotopy analysis scheme [25-30]. The solution convergence is also examined. The flow parameters for velocity, temperature and concentration are discussed with physical applications.

Mathematical modelling

Let us develop a nanofluid model for Oldroyd-fluid by utilizing the thermal slip features. The non-Newtonian fluid is confined between stretchable disks where flow is imagined to be 2-D. At the surfaces of disks, the velocity and thermal slip constraints are elaborated. The magnetic force consequences has been reported along-axis. The temperature at lower surface of disk is while is upper surface temperature. The famous cylindrical axes and are followed to model the problem. Due to the axisymmetry constraints, the physical quanties are free of The equations for Oldroyd-B liquid with impact of magnetic force, nanoparticles and thermophoresis features are expressed [8]:

$$\frac{1}{r}\frac{\partial}{\partial r}(ru)+\frac{\partial w}{\partial z}=0 \tag{1}$$

$$u\frac{\partial u}{\partial r}+w\frac{\partial u}{\partial z}=-\frac{1}{\rho}\frac{\partial p}{\partial r}+\nu\left(2\frac{\partial^2 u}{\partial r^2}+\frac{\partial^2 w}{\partial r\partial z}+\frac{\partial^2 u}{\partial z^2}+\frac{2}{r}\frac{\partial u}{\partial r}-2\frac{u}{r^2}\right)-$$
$$-\beta_1^*\left(w^2\frac{\partial^2 u}{\partial z^2}+2uw\frac{\partial^2 u}{\partial r\partial z}+\frac{\partial^2 u}{\partial r^2}\right)+\nu\beta_2^*\left[\frac{4u^2}{r^3}-\frac{2w}{r^2}\frac{\partial u}{\partial z}-\frac{1}{r}\left(\frac{\partial u}{\partial z}\right)^2-\right.$$
$$-2\frac{\partial u}{\partial z}\frac{\partial^2 w}{\partial z^2}+w\frac{\partial^3 u}{\partial z^3}-\frac{2u}{r^2}\frac{\partial u}{\partial r}-\frac{\partial^2 u}{\partial z^2}\frac{\partial u}{\partial r}-\frac{2}{r}\left(\frac{\partial u}{\partial r}\right)^2-\frac{1}{r}\frac{\partial u}{\partial z}\frac{\partial w}{\partial r}+\frac{2w}{r}\frac{\partial^2 u}{\partial r\partial z}-$$
$$-\frac{\partial u}{\partial z}\frac{\partial^2 u}{\partial r\partial z}-\frac{\partial u}{\partial r}\frac{\partial^2 w}{\partial r\partial z}+u\frac{\partial^3 u}{\partial r\partial z^2}+w\frac{\partial^3 w}{\partial r\partial z^2}+\frac{2u}{r}\frac{\partial^2 u}{\partial r^2}-2\frac{\partial u}{\partial r}\frac{\partial^2 u}{\partial r^2}-$$
$$\left.-\frac{\partial u}{\partial z}\frac{\partial^2 w}{\partial r^2}+2w\frac{\partial^3 u}{\partial r^2\partial z}+u\frac{\partial^3 w}{\partial r^2\partial z}+2u\frac{\partial^3 u}{\partial r^3}\right]+\frac{\sigma {B_0}^2}{\rho}\left(-u-\beta_1^* w\frac{\partial u}{\partial z}\right) \tag{2}$$

$$u\frac{\partial w}{\partial r}+w\frac{\partial w}{\partial z}=-\frac{1}{\rho}\frac{\partial p}{\partial z}+\nu\left(\frac{\partial^2 w}{\partial r^2}+\frac{\partial^2 u}{\partial r\partial z}+2\frac{\partial^2 w}{\partial z^2}+\frac{1}{r}\frac{\partial w}{\partial r}+\frac{1}{r}\frac{\partial u}{\partial r}\right)-$$
$$-\beta_1^*\left(w^2\frac{\partial^2 u}{\partial z^2}+2uw\frac{\partial^2 u}{\partial r\partial z}+u^2\frac{\partial^2 u}{\partial r^2}\right)+\nu\beta_2^*\left(-\frac{u}{r^2}\frac{\partial u}{\partial z}-\frac{1}{r}\frac{\partial u}{\partial z}\frac{\partial w}{\partial z}+\frac{w}{r}\frac{\partial^2 u}{\partial z^2}-\right.$$
$$-2\frac{\partial w}{\partial z}\frac{\partial^2 w}{\partial z^2}+2w\frac{\partial^3 w}{\partial z^3}+-\frac{u}{r^2}\frac{\partial w}{\partial r}-\frac{1}{r}\frac{\partial w}{\partial r}\frac{\partial w}{\partial z}-\frac{\partial^2 u}{\partial z^2}\frac{\partial w}{\partial r}-\frac{2}{r}\frac{\partial u}{\partial r}\frac{\partial w}{\partial r}+\frac{u}{r}\frac{\partial^2 u}{\partial r\partial z}-$$
$$-\frac{\partial w}{\partial z}\frac{\partial^2 u}{\partial r\partial z}+\frac{w}{r}\frac{\partial^2 w}{\partial r\partial z}-\frac{\partial w}{\partial r}\frac{\partial^2 w}{\partial r\partial z}+w\frac{\partial^3 u}{\partial r\partial z^2}+2u\frac{\partial^3 w}{\partial r\partial z^2}\left.\right)-2\frac{\partial w}{\partial r}\frac{\partial^2 u}{\partial r^2}+$$
$$+\frac{u}{r}\frac{\partial^2 w}{\partial r^2}-\frac{\partial w}{\partial z}\frac{\partial^2 w}{\partial r^2}+u\frac{\partial^3 u}{\partial r^2\partial z}+w\frac{\partial^3 w}{\partial r^2\partial z}+u\frac{\partial^3 w}{\partial r^3} \tag{3}$$

$$u\frac{\partial T}{\partial r}+w\frac{\partial T}{\partial z}=\alpha\left(\frac{\partial^2 T}{\partial r^2}+\frac{1}{r}\frac{\partial T}{\partial r}+\frac{\partial^2 T}{\partial z^2}\right)+\tau\left[D_B\left(\frac{\partial C}{\partial r}\frac{\partial T}{\partial r}+\frac{\partial C}{\partial z}\frac{\partial T}{\partial z}\right)+\right.$$
$$\left.+\frac{D_T}{T_m}\left\{\left(\frac{\partial T}{\partial r}\right)^2+\left(\frac{\partial T}{\partial r}\right)^2\right\}\right]+Qk_0a_0\mathrm{e}^{-E/R_1T} \tag{4}$$

$$u\frac{\partial C}{\partial r}+w\frac{\partial C}{\partial z}=D_B\left(\frac{\partial^2 C}{\partial r^2}+\frac{1}{r}\frac{\partial C}{\partial r}+\frac{\partial^2 C}{\partial z^2}\right)+\frac{D_T}{T_m}\left(\frac{\partial^2 T}{\partial r^2}+\frac{1}{r}\frac{\partial T}{\partial r}+\frac{\partial^2 T}{\partial z^2}\right)-\frac{\partial\left[V_T\left(C-C_1\right)\right]}{\partial z} \tag{5}$$

The slip boundary conditions for formulated flow problem:

$$\begin{aligned}u&=ar+\left(\frac{2-\sigma_u}{\sigma_u}\right)\tau_1\frac{\partial u}{\partial z}+\left(\frac{2-\sigma_u}{\sigma_u}\right)\tau_1^2\frac{\partial^2 u}{\partial z^2},\ \ w=0,\ \ p=\frac{a\mu\beta_1 r^2}{4d^2},\ \ \text{at}\ \ z=0\\ u&=cr-\left(\frac{2-\sigma_u}{\sigma_u}\right)\tau_1\frac{\partial u}{\partial z}-\left(\frac{2-\sigma_u}{\sigma_u}\right)\tau_1^2\frac{\partial^2 u}{\partial z^2},\ \ w=0,\ \ p=0,\ \ \text{at}\ \ z=d\end{aligned} \tag{6}$$

Similarly the boundary conditions for nanoparticles temperature are also imposed in form of following jump slip relations:

$$T=T_1+\left(\frac{2-\sigma_T}{\sigma_T}\right)\left(\frac{2\xi}{\xi+1}\right)\frac{1}{\mathrm{Pr}}\tau_2\frac{\partial T}{\partial z}+\left(\frac{2-\sigma_T}{\sigma_T}\right)\left(\frac{2\xi}{\xi+1}\right)\frac{1}{\mathrm{Pr}}\frac{\tau_2^2}{2}\frac{\partial^2 T}{\partial z^2},\ \ \text{at}\ \ z=0 \tag{7}$$

$$T=T_2-\left(\frac{2-\sigma_T}{\sigma_T}\right)\left(\frac{2\xi}{\xi+1}\right)\frac{1}{\mathrm{Pr}}\tau_2\frac{\partial T}{\partial z}+\left(\frac{2-\sigma_T}{\sigma_T}\right)\left(\frac{2\xi}{\xi+1}\right)\frac{1}{\mathrm{Pr}}\frac{\tau_2^2}{2}\frac{\partial^2 T}{\partial z^2},\ \ \text{at}\ \ z=d \tag{8}$$

The nanoparticles concentration is reported by using following no-slip conditions:

$$C=C_1,\ \ z=0,\ \ C=C_2\ \ \text{at}\ z=d \tag{9}$$

The physical quantities are radial component, u, axial component, w, pressure, p, fluid density, ρ, dynamic viscosity, μ, kinematic viscosity, ν, relaxation time, β_1^*, retardation time β_2^*, temperature, T, thermal diffusivity, K, concentration, C, thermophoretic coefficient, D_T, mean temperature, T_m, thermophoretic velocity, V_T, Brown diffusion coefficient, D_B, thermal accommodation coefficient, σ_T, specific heat ratio, ξ, stretching rates constants, a and b, tangential momentum accommodation constant, σ_u, and molecular mean path, τ_1.

The dimensionless form of given equations can be resulted via relations [8]:

$$\begin{aligned}u&=-\frac{ar}{2}H'(\eta),\ \ w=adH(\eta),\ \ p=a\mu\left[P(\eta)+\frac{\beta_1 r^2}{4d^2}\right],\ \ \eta=\frac{z}{d}\\ T&=T_1+\left(T_2-T_1\right)\theta(\eta),\ \ C=C_1+\left(C_2-C_1\right)\varphi(\eta)\end{aligned} \tag{10}$$

After altering these relations, set of dimensionless equations is obtained:

$$\frac{\mathrm{Re}}{2}\left(H'^2-2HH''\right)=-\left\{\beta_1+H'''+\lambda_1'a\,\mathrm{Re}\left(HH'H''-H^2H'''\right)+\lambda_2'a\left[HH^{(iv)}-H''^2\right]\right\}+$$
$$+\mathrm{Re}\,\mathrm{M}\left(H'+\lambda_1'aHH''\right) \tag{11}$$

$$\theta''-\mathrm{Re}\,\mathrm{Pr}H\theta'+Nb\mathrm{Pr}\theta'\varphi'+Nt\mathrm{Pr}\varepsilon\theta'^2+K\exp\left[\frac{-1}{\varepsilon\left(1+\varepsilon\theta\right)}\right]=0 \tag{12}$$

$$\varphi'' - \mathrm{Re}\,\mathrm{LePr}H\varphi' + \left(\frac{Nt}{Nb}\right)\varepsilon\theta'' + J\mathrm{LePr}\varepsilon\left(\theta'\varphi' + \varphi\theta''\right) = 0 \tag{13}$$

$$P' = \frac{3H''}{2} - \mathrm{Re}\,HH' - \lambda_1\,\mathrm{Re}\,H^2H'' \tag{14}$$

$$H(0) = 0,\ \ H(1) = 0,\ \ H'(0) = -2 + \left[\varepsilon_1 H''(0) + \varepsilon_2 H'''(0)\right] \tag{15}$$

$$H'(1) = -2\gamma - \left[\varepsilon_1 H''(0) + \varepsilon_2 H'''(0)\right],\ \ P(0) = 0 \tag{16}$$

$$\theta(0) = \varepsilon_3\theta'(0) + \varepsilon_4\theta''(0),\ \ \theta(1) = 1 - \left[\varepsilon_3\theta'(1) + \varepsilon_4\theta''(1)\right] \tag{17}$$

$$\varphi(0) = 0,\ \ \varphi(1) = 1 \tag{18}$$

The dimension variables are Reynolds number, Re, Deborah number for relaxation, λ_1, retardation time, λ_2, wall stretching parameter, γ, first order velocity slip, ε_1, Hartmann number, M, Prandtl number, Pr, second order velocity slip parameter, ε_2, first order temperature jump parameter, ε_3, temperature jump parameter of second order, ε_4, Schmidt number, Sc, ratio of diffusion coefficient, δ, and Knudsen number, Kn, which are defined:

$$\gamma = \frac{c}{a},\ \lambda_1 = \beta_1^* a,\ \mathrm{Re} = \frac{ad^2}{\nu},\ \mathrm{Pr} = \frac{\nu}{\alpha},\ \mathrm{Kn} = \frac{\tau_{1,2}}{d}$$

$$\lambda_2 = \beta_2^* a,\ \varepsilon_1 = \mathrm{Kn}\left(\frac{2-\sigma_u}{\sigma_u}\right),\ \ \varepsilon_2 = \frac{\mathrm{Kn}^2}{2}\left(\frac{2-\sigma_u}{\sigma_u}\right)$$

$$\varepsilon_3 = \mathrm{Kn}\left(\frac{2-\sigma_T}{\sigma_T}\right)\left(\frac{2\xi}{\xi+1}\right)\frac{1}{\mathrm{Pr}},\ \varepsilon_4 = \frac{\mathrm{Kn}^2}{2}\left(\frac{2-\sigma_T}{\sigma_T}\right)\left(\frac{2\xi}{\xi+1}\right)\frac{1}{\mathrm{Pr}},\ \delta = \frac{D_B}{D_A}$$

From eq. (17), the constant β_1 is illuminated:

$$\begin{aligned} H^{(iv)} &= \mathrm{Re}\,HH''' - \lambda_1\,\mathrm{Re}\left[-HH'H''' - H^2H^{(iv)} + HH''^2 + H'^2H''\right] - \\ &-\mathrm{M}\,\mathrm{Re}\left[H'' + \lambda_1\left(H'H'' + HH'''\right)\right] - \lambda_2\left[-2H''H''' + H'H^{(iv)} + HH^{(v)}\right] \end{aligned} \tag{19}$$

Following mathematical expressions are notified to explore the numerical features of skin friction coefficient, Sherwood number and Nusselt number confined at both disks walls:

$$C_{1f,2f} = \frac{\tau_{rz}\,|_{\eta=0,1}}{\frac{1}{2}\rho(\delta r)^2} = 2\,\mathrm{Re}^{-1}H''(\eta)\Big|_{\eta=0,1},\ N_{1u,2u} = -\frac{\mathrm{d}k_T\frac{\partial T}{\partial z}|_{\eta=0,1}}{k_T\left(T_2 - T_1\right)} = -\theta'(\eta)\Big|_{\eta=0,1} \tag{20}$$

$$\mathrm{Sh} = \frac{-\left(D\frac{\partial C}{\partial z}\right)\Big|_{\eta=0,1}}{D\left(C_1 - C_2\right)} = -\varphi'(\eta)\Big|_{\eta=0,1} \tag{21}$$

Method of solution

The initial approximations in following forms are suggested to start the simulation procedure:

$$H_0(\eta)=\frac{1}{8\varepsilon_1+12\varepsilon_1^2}\left(-2\eta(1+\eta)\left\{-1+\eta(1+\gamma)+2\varepsilon_1\left[-2+\eta+\gamma(1+\eta)\right]-6\varepsilon_2(1+\eta)\right\}\right) \tag{22}$$

$$\theta_0(\eta)=\frac{\eta+\varepsilon_3}{1+2\varepsilon_3},\ \ \varphi_0(\eta)=\eta \tag{23}$$

along with linear operators:

$$L_H=\frac{\mathrm{d}^4}{\mathrm{d}\eta^4},\ L_\theta=\frac{\mathrm{d}^2}{\mathrm{d}\eta^2},\ L_\varphi=\frac{\mathrm{d}^2}{\mathrm{d}\eta^2} \tag{24}$$

The approximations for zeroth- order are developed:

$$(1-q)L_H\left[H(\eta;q)-H_0(\eta)\right]=q\hbar_H N_H\left[H(\eta;q)\right] \tag{25}$$

$$(1-q)L_\theta\left[\theta(\eta;q)-\theta_0(\eta)\right]=q\hbar_\theta N_\theta\left[\theta(\eta;q)\right] \tag{26}$$

$$(1-q)L_\varphi\left[\varphi(\eta;q)-\varphi_0(\eta)\right]=q\hbar_\varphi N_\varphi\left[\varphi(\eta;q)\right] \tag{27}$$

The m^{th} order problem:

$$L_H\left[H_m(\eta)-\chi_m H_{m-1}(\eta)\right]=\hbar_H\,\mathrm{Re}_{1m}(\eta) \tag{28}$$

$$L_\theta\left[\theta_m(\eta)-\chi_m\theta_{m-1}(\eta)\right]=\hbar_\theta\,\mathrm{Re}_{2m}(\eta) \tag{29}$$

$$L_\varphi\left[\varphi_m(\eta)-\chi_m\varphi_{m-1}(\eta)\right]=\hbar_\varphi\,\mathrm{Re}_{3m}(\eta) \tag{30}$$

$$H_m(0)=H_m(1)=0\ \ H_m'(0)=\left[\varepsilon_1 H_m''(0)+\varepsilon_2 H_m'''(0)\right],\ \ H_m'(1)=-\left[\varepsilon_1 H_m''(1)+\varepsilon_2 H_m'''(1)\right] \tag{31}$$

$$\theta_m(0)=\left[\varepsilon_3\theta_m'(0)+\varepsilon_4\theta_m''(0)\right],\ \ \theta(1)=-\left[\varepsilon_3\theta_m'(1)+\varepsilon_4\theta_m''(1)\right] \tag{32}$$

$$\varphi_m(0)=0,\ \ \varphi_m(1)=1 \tag{33}$$

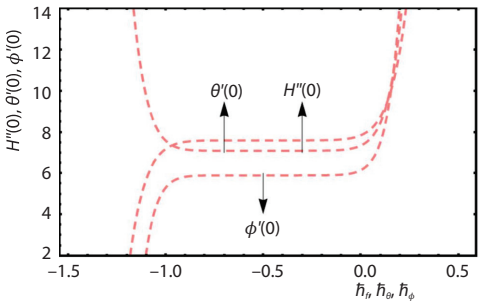

Figure 1. The $\hbar$-curves for velocity temperature and concentration profiles

$$\chi_m=\begin{cases}0, & m\le 1\\ 1, & m>0\end{cases} \tag{34}$$

The computation software MATHEMATICA help out to facilitate the simulation procedure.

Convergence of solution

After obtaining the analytical expressions successfully, aim of this section report the convergent analysis which has key importance in adopted convergent technique. The auxiliary parameters ($\hbar_H$, $\hbar_\theta$, $\hbar_\varphi$) are play a diligent contribu-

tion suggest the convergence procedure. The necessary $\hbar$-curves are constructed for velocity, temperature and concentration distributions are prepared under the specific values of parameters. The guaranteed convergence region is result under set of flow parameters. Figure 1 reports such convergence values which reveal that best convergence solution is associated with domain $-1 \leq \hbar_H \leq -0.1$, $-1.3 \leq \hbar_\theta \leq -0.2$, and $-1.2 \leq \hbar_\varphi \leq -0.1$ The convergence analysis for $H''(0)$, $\theta'(0)$, $\varphi'(0)$ is worked out in tab. 1 which shows that convergence of numerical values is achieved at 13th order of approximations.

Table 1. The HAM convergence at different order of approximations

Approximation	$H''(0)$	$\theta'(0)$	$\varphi'(0)$
5	6.66130	0.446623	0.243144
10	6.66121	0.446434	0.242136
12	6.65118	0.446334	0.242128
15	6.65110	0.446200	0.242120
20	6.65110	0.446200	0.242120

Discussion

The physical consequences for a model flow problem are quite necessary to see the clear insight flow problem [31-34]. Now the physical aspects of flow problem against parameters are studied in this section. The graphical simulations are prepared in view of flow constraints parameters against velocity, temperature, and concentration which are already altered in dimensionless forms. The whole analysis is performed by keeping fixed values like Re = 0.5,

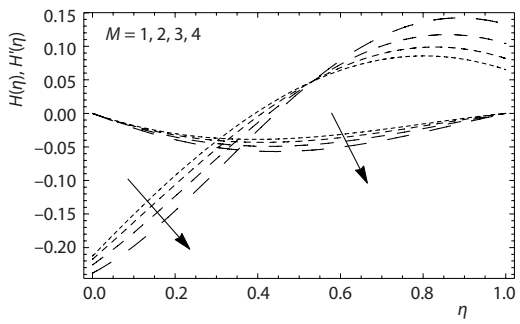

Figure 2. Velocity components for M

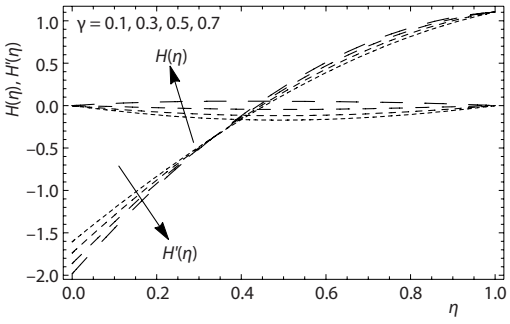

Figure 3. Velocity components for γ

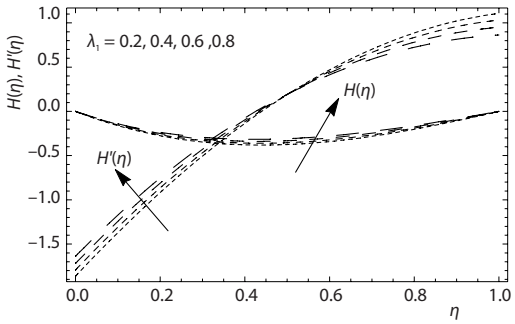

Figure 4. Velocity components for λ_1

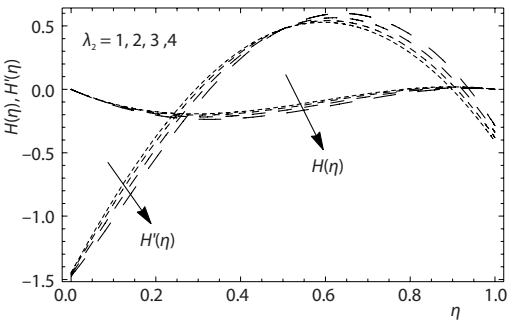

Figure 5. Velocity components for λ_2

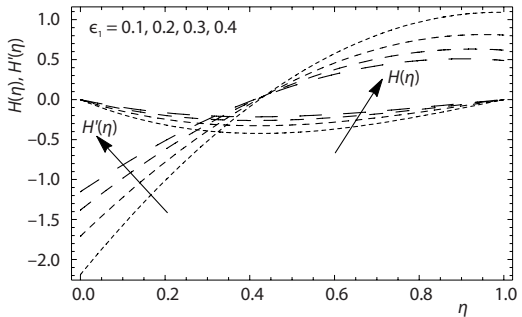

Figure 6. Velocity components for ε_1

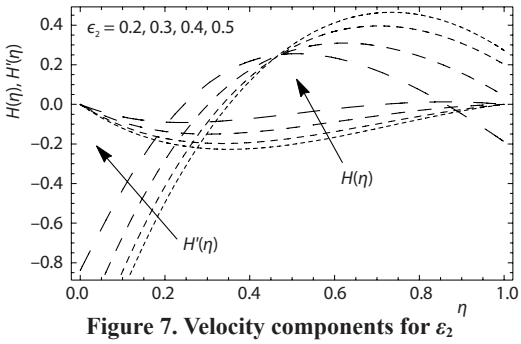

Figure 7. Velocity components for ε_2

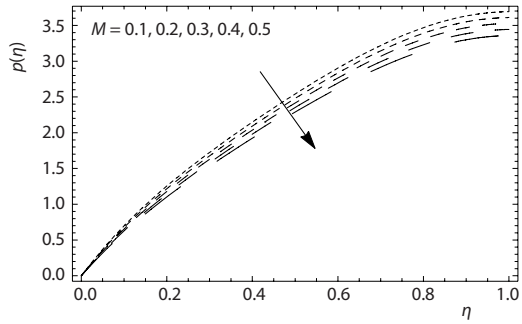

Figure 8. Change in pressure with M

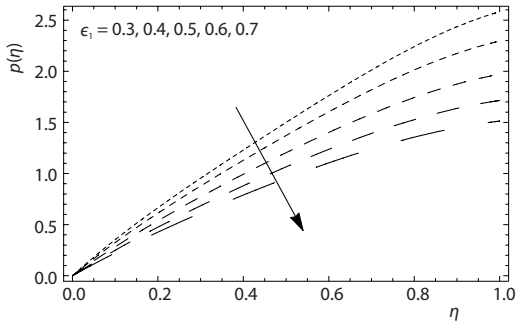

Figure 9. Change in pressure with ε_1

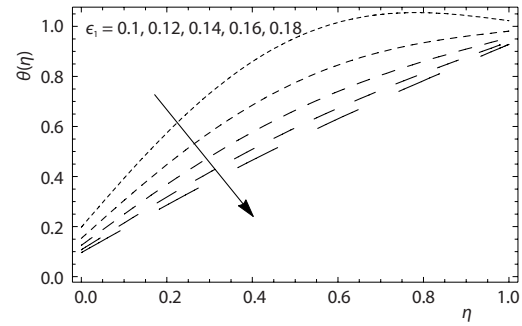

Figure 10. Change in temperature with ε_1

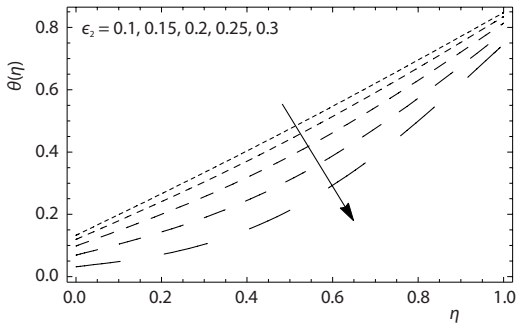

Figure 11. Change in temperature with ε_2

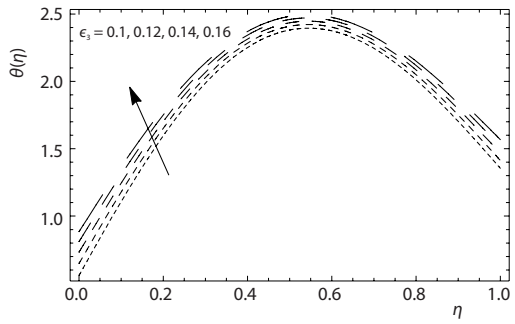

Figure 12. Change in temperature with ε_3

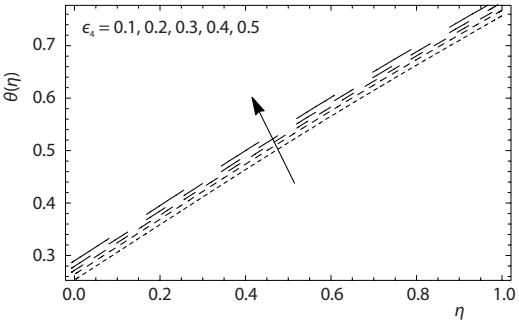

Figure 13. Change in temperature with ε_4

$\gamma = 0.2$, M = 0.5, $Nb = 0.2$, Pr = 0.1, $\lambda_1 = 0.2$, $\lambda_2 = 0.1$, $\varepsilon_1 = 0.2$, $\varepsilon_2 = 0.3$, $\varepsilon_3 = 0.3$, and $\varepsilon_4 = 0.5$. Figure 2 communicates the influence Hartmann number on radial and vertical velocity components. Due to resistance of Lorentz force associated with larger magnetic field result a decrement in velocity components up to a specific level. The plot for wall stretching constant, γ, against the radial and vertical velocities is prepared in fig. 3. Here a rise in both components notified with larger γ variation. The curve for relaxation constant, λ_1, and retardation constant, λ_2, are plotted in figs. 4 and 5, respectively. An improve velocity distributions is associated with λ_1 in contrast to λ_2. Physically, with increment of relaxation time parameter, more time needed to retain the fluid original position. A lower distribution of radial and vertical components are noticed when λ_2 is maximum. In fig. 6, the output of fist order velocity slip constant ε_1 is suggested for velocity components. Both components increases when ε_1 is larger varies. The opposite observations are specified for ε_2 and examined by plotting fig. 7. Figures 8 and 9 report the change in pressure distribution for Hartmann number and ε_1, respectively. With larger assigns values to both Hartmann number and ε_1, the pressure distribution declined. However, the change in pressure is comparatively dominant for slip constant ε_1. Figures 10 and 11 give the temperature distribution, θ, for velocity slip parameters ε_1 and ε_2. The observations claim a lower temperature profile with both parameters. The change in θ due to thermal slip parameters ε_3 and ε_4 is reported

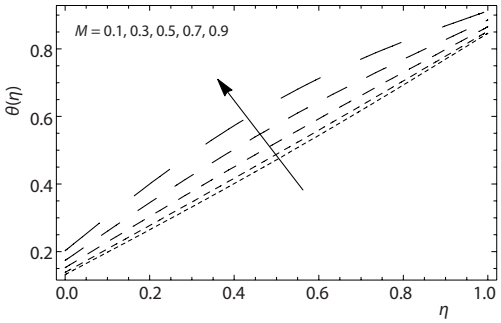

Figure 14. Change in temperature with M

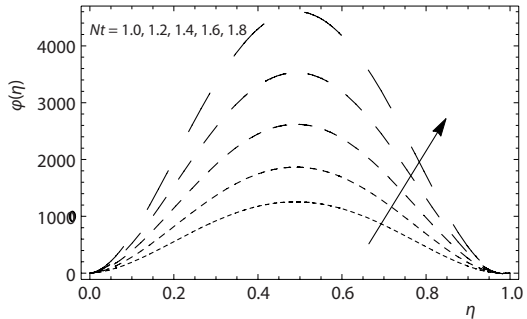

Figure 15. Change in concentration with *Nt*

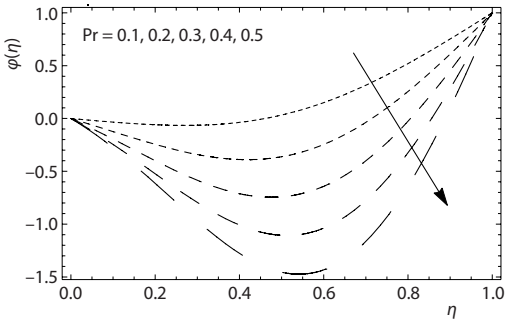

Figure 16. Change in concentration with Pr

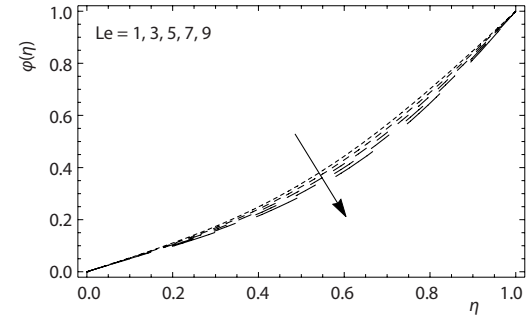

Figure 17. Change in concentration with Le

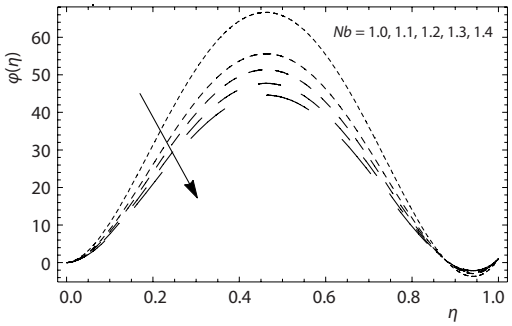

Figure 18. Change in concentration with *Nb*

by preparing figs. 12 and 13. Here, an increasing trend is noted for θ for both constants. Therefore, it is remarked that consideration of thermal slip features are more effective to improve the heat transportation processes. The graphical results for Hartmann number are reported in fig. 14. The nanoparticles temperature is increasing when Hartmann number is maximum. Physical larger values of Hartmann number are associated with Lorentz force which increase the temperature. The results utilizes figs. 15-18 determine the change in nanoparticles concentration, φ, with numerous values of thermophoresis parameter, *Nt*, Prandtl number, Lewis number, and Brownian motion constant, *Nb*. From fig. 15, upshot concentration distribution is observed when *Nt* is maximum. Physically, thermophoresis phenomenon represents the migration pattern of heated fluid particles towards the cold region. Due to this, temperature increases. The results reported in fig. 16 claim that concentration reduces with upshot values of Prandtl number. Figure 17 aim to presents the novel impact of Lewis number on φ. Here the results claim a reduce nanoparticles concentration for Lewis number. Physically the Lewis number is inversely related to mass diffusivity due to higher Lewis number. Figure 18 presents the influence of *Nb* on φ. As expected, concentration is lower for *Nb*.

The numerical expression based on the Nusselt number is evaluated in tab. 2. At lower disk surface, the heat transfer is minimum for Hartmann number. However, the upper wall show an increasing variation. The Nusselt number decreases for velocity slip parameter.

Table 2. The variation of Nusselt number with different parameters

ε_1	ε_2	ε_3	ε_4	Pr	M	Lower disk	Upper disk
0.2	0.5	0.5	0.2	1.0	0.3	–0.62653	–0.72854
0.4	0.5	0.5	0.2	1.0	0.3	–0.60435	–0.71095
0.6	0.5	0.5	0.2	1.0	0.3	–0.54675	–0.70462
0.2	0.1	0.5	0.2	1.0	0.3	–0.64478	–0.70741
0.2	0.3	0.5	0.2	1.0	0.3	–0.55535	–0.63751
0.2	0.6	0.5	0.2	1.0	0.3	–0.37754	–0.45679
	0.5	0.1	0.2	1.0	0.3	–0.60753	–0.63975
	0.5	0.3	0.2	1.0	0.3	–0.69278	–0.70568
	0.5	0.6	0.2	1.0	0.3	0.80549	–0.80653
	0.5	0.5	0.5	1.0	0.3	–0.54546	–0.44705
	0.5	0.5	1.0	1.0	0.3	–0.54587	–0.44764
	0.5	0.5	2.0	1.0	0.3	–0.54546	–0.44654
	0.5	0.5	0.2	0.2	0.3	–0.47742	–0.52534
	0.5	0.5	0.2	0.4	0.3	–0.47667	–0.52364
	0.5	0.5	0.2	0.6	0.3	–0.47522	–0.52457
	0.5	0.5	0.2	1.0	0.3	–0.47653	–0.54575
	0.5	0.5	0.2	1.0	0.5	–0.48984	–0.52653
	0.5	0.5	0.2	1.0	0.7	–0.49458	–0.50905

Conclusions

The rheological consequences for Oldroyd-B nanofluid is studies in presence of velocity and thermal slip features. The modeled flow problem is analytically tackled via homotopy analysis method. The convergence procedure is followed to confirm the solution. The main results are as follows.

- The stretching ratio constant increases the radial and normal velocity components.
- An increment in radial and normal velocity components are noted for velocity slip parameters.

- The Hartmann number effectively controls the fluid particles movement at both surfaces of disks.
- A declining temperature distribution is observed for velocity slip parameters.
- The nanoparticles temperature can be enhanced with proper utilization thermal slip constants.
- The concentration profile is lower for Brownian motion constant, Lewis number and Prandtl number.
- The thermophoresis constant improve the nanoparticles concentration effectively.

Acknowledgment

The authors would like to acknowledge Natural Science Foundation of China (Grant No. 61673169, 11701176, 11626101, and 11601485).

References

[1] Karman, V., Uber, T., Laminar und Turbulente Reibung (in German), *Zeitschrift f˙ur Angewandte Mathematic and Mechanik (ZAMM)*, *1* (1921), 4, pp. 233-255
[2] Hayat, T., *et al*., The MHD Axisymmetric Flow of Third Grade Fluid between Porous Disks with Heat Transfer (ed. English), *Applied Mathematicsand Mechanics*, *33* (2012), 6, pp. 749-764
[3] Turkyilmazoglu, M., The 3-D MHD Stagnation Flow Due to a Stretchable Rotating Disk, *International Journal of Heat and Mass Transfer*, *55* (2012), 23-24, pp. 6959-6965
[4] Turkyilmazoglu, M., The MHD Fluid-Flow and Heat Transfer Due to a Shrinking Rotating Disk, *Computers and Fluids*, *90* (2014), Feb., pp. 51-56
[5] Soid, S. K., *et al*., The MHD Flow and Heat Transfer over a Radially Stretching/Shrinking Disk, *Chinese Journal of Physics*, *56* (2018), 1, pp. 58-66
[6] Yin, C., *et al*., Flow and Heat Transfer of Nanofluids over a Rotating Disk with Uniform Stretching Rate in the Radial Direction, *Propulsion and Power Research*, *6* (2017), 1, pp. 25-30
[7] Turkyilmazoglu, M., Fluid-Flow and Heat Transfer over a Rotating and Vertically Moving Disk, *Physics of Fluids*, *30* (2018), 6, 063605
[8] Hashmi, M. S., *et al*., A Mathematical Model for Mixed Convective Flow of Chemically Reactive Oldroyd-B Fluid between Isothermal Stretching Disks, *Results in Physics*, *7* (2017), Aug., pp. 3016-3023
[9] Rashidi, M. M., *et al*., Simultaneous Effects of Partial Slip and Thermal-Diffusion and Diffusion-Thermo on Steady MHD Convective Flow Due to a Rotating Disk, *Communications in Non-linear Science and Numerical Simulation*, *16* (2011), 11, pp. 4303-4317
[10] Khan, N., *et al*., Flow of a Hydromagnetic Viscous Fluid between Parallel Disks with Slip, *Journal of Mechanics*, *31* (2015), 6, pp. 713-726
[11] Khan, N., *et al*., Heat Transfer Analysis for Magnetohydrodynamics Axi-Symmetric Flow between Stretching Disks in the Presence of Viscous Dissipation and Joule Heating, *AIP Advances*, *5* (2015), 057115
[12] Zheng, L., *et al*., Exact Solutions for MHD Flow of Generalized Oldroyd-B Fluid Due to an Infinite Accelerating Plate, *Mathematical and Computer Modelling*, *54* (2011), 1-2, pp. 780-788
[13] Hayat, T., *et al*., Stretched Flow of Oldroyd-B Fluid with Cattaneo-Christov Heat Flux, *Results in Physics*, 7 (2017), July, pp. 2470-2476
[14] Zheng, L., *et al*., Slip Effects on MHD Flow of a Generalized Oldroyd-B Fluid with Fractional Derivative, *Non-Linear Analysis: Real World Applications*, *13* (2012), 2, pp. 513-523
[15] Chiu, S., *et al*., A 3-D DLM/FD Method for Simulating the Motion of Spheres in a Bounded Shear Flow of Oldroyd-B Fluids, *Computers and Fluids*, *172* (2018), Aug., pp. 661-673
[16] Farooq, A., *et al*., Soret and Dufour Effects on 3-D Oldroyd-B Fluid, *Physica A: Statistical Mechanics and its Applications*, *503* (2018), Aug., pp. 345-354
[17] Ali, F., *et al*., Application of Caputo-Fabrizio Derivatives to MHD Free Convection Flow of Generalized Walters-B Fluid Model, *The European Physical Journal Plus*, *131* (2016), 377
[18] Ali, F., *et al*., Magnetic Field Effect on Blood Flow of Casson Fluid in Axisymmetric Cylindrical Tube: A Fractional Model, *Journal of Magnetism and Magnetic Materials*, *423* (2017), Feb., pp. 327-336
[19] Samiulhaq, A. S., *et al*., Unsteady Magneto Hydrodynamic Free Convection Flow of a Second Grade Fluid in a Porous Medium with Ramped Wall Temperature, PLoS One, *9* (2014), e88766

[20] Raza, J., *et al*., Magnetohydrodynamic Flow of Nano Williamson Fluid Generated by Stretching Plate with Multiple Slips, *Multidiscipline Modelling in Materials and Structures*, *15* (2019), 5, pp. 871-894
[21] Raza, J., *et al*., Multiple Slip Effects on MHD Non-Newtonian Nanofluid-Flow over a Non-Linear Permeable Elongated Sheet: Numerical and Statistical Analysis, *Multidiscipline Modelling in Materials and Structures*, *15* (2019), 5, pp. 913-931
[22] Mahanthesh, B., *et al*., Significance of Exponential Space- and Thermal-Dependent Heat Source Effects on Nanofluid-Flow Due to Radially Elongated Disk with Coriolis and Lorentz Forces, *Journal Therm. Anal Calorim*, *141* (2020), Nov., pp. 37-44
[23] Mebarek-Oudina F., Convective Heat Transfer of Titania Nanofluids of Different Base Fluids in Cylindrical Annulus with Discrete Heat Source, *Heat transfer Asian Research*, *48* (2019), 1, pp. 135-147
[24] Alkasassbeh, M., *et al*., Heat Transfer Study of Convective Fin with Temperature-Dependent Internal Heat Generation by Hybrid Block Method, *Heat transfer Asian Research*, *48* (2019), 4, pp. 1225-1244
[25] Liao, S. J., *Advance in the Homotopy Analysis Method*, 5 Toh Tuck Link, World Scientific Publishing Singapore, Singapore, 2014
[26] Khan, S. U., *et al*., Soret and Dufour Effects on Hydromagnetic-Flow of Eyring Powell Fluid over an Oscillatory Stretching Surface with Heat Generation/Absorption and Chemical Reaction, *Thermal Science*, *22* (2018), 1B, pp. 533-543
[27] Hussain,T., *et al*., Impact of Magnetic Field in Radiative Flowof Casson Nanofluid with Heat and Mass Fluxes, *Thermal Science*, *22* (2018), 1A, pp. 137-145
[28] Khan, S. U., *et al*., Heat Transfer Analysis Based on Cattaneo-Christov Model and Convective Boundary Conditions for Flow over an Oscillatory Stretching Surface: A Mathematical Model, *Thermal Science*, *23* (2019), 2A, pp. 443-455
[29] Turkyilmazoglu, M., Solution of the Thomas-Fermi Equation with a Convergent Approach, *Communications in Non-Linear Science and Numerical Simulation*, *17* (2012), 11, pp. 4097-4103
[30] Turkyilmazoglu, M., Parametrized Adomian Decomposition Method with Optimum Convergence, *ACM Transactions on Modelling and Computer Simulation*, *27* (2017), Oct., pp. 1-22
[31] Inc, M., *et al*., Modified Variational Iteration Method for Straight Fins with Temperature Dependent Thermal Conductivity, *Thermal Science*, *22* (2018), Suppl. 1, pp. S229-S236
[32] Kilicman, A., *et al*., Analytic Approximate Solutions for Fluid-Flow in the Presence of Heat and Mass, *Thermal Science*, *22* (2018), Suppl. 1, pp. S259-S264
[33] Inc, M., Application of Homotopy Analysis Method for Fin Efficiency of Convective Straight Fins with Temperature-Dependent Thermal Conductivity, *Math. Computer Sim*., *79* (2008), 2, pp. 189-200
[34] Hashemi, M. S., *et al*., On Fractional kdv-Burgers and Potential kdv Equations: Existence and Uniqueness Results, *Thermal Science*, *23* (2019), Suppl. 1, pp. S2107 - S2117

Paper submitted: March 5, 2020
Paper revised: May 30, 2020
Paper accepted: June 12, 2020

© 2020 Society of Thermal Engineers of Serbia
Published by the Vinča Institute of Nuclear Sciences, Belgrade, Serbia.
This is an open access article distributed under the CC BY-NC-ND 4.0 terms and conditions